Electroweak Physics, QCD and Jets in the Forward Region

Chiapolini, N

Abstract: The LHCb experiment has successfully taken data during the last three years. Here, results are presented for W, Z and low mass Drell–Yan production in the forward region at LHCb. Analyses based on data collected in 2010 and 2011 are presented. The results are generally in agreement with theoretical predictions.

DOI: https://doi.org/10.5506/APhysPolB.44.1385

ELECTROWEAK PHYSICS, QCD AND JETS IN THE FORWARD REGION*

Nicola Chiapolini

for the LHCb Collaboration

Physik-Institut der Universität Zürich
Winterthurerstrasse 190, 8057 Zürich, Switzerland

(Received April 16, 2013)

The LHCb experiment has successfully taken data during the last three years. Here, results are presented for W, Z and low mass Drell–Yan production in the forward region at LHCb. Analyses based on data collected in 2010 and 2011 are presented. The results are generally in agreement with theoretical predictions.

DOI:10.5506/APhysPolB.44.1385
PACS numbers: 12.15.–y, 13.87.–a, 14.70.Fm, 14.70.Hp

1. Introduction

The LHCb experiment [1] is one of the four experiments at the Large Hadron Collider (LHC). It is designed to perform CP violation and rare decay studies in the heavy quark sector. It also provides important contributions to the understanding of electroweak processes at LHC energies such as W, Z and Drell–Yan production. The LHCb detector is a single-arm forward spectrometer, with a pseudorapidity coverage of $2 < \eta < 5$. The LHCb experiment is able to trigger on particles down to transverse momenta of a few GeV/c. This allows the measurement of the low mass Drell–Yan production. The experiment has successfully taken data during the last three years. In 2010 and 2011, LHC ran at a centre-of-mass energy of 7 TeV. The integrated luminosity acquired by the experiments was 37 pb^{-1} and 1.1 fb^{-1}, respectively. All measurements reported here use these data. In 2012, the experiment collected 2.1 fb^{-1} at 8 TeV. These data are not yet analysed. During the full data taking period, the average number of interactions per bunch crossing stayed roughly constant at 1.5.

* Presented at the Cracow Epiphany Conference on the Physics After the First Phase of the LHC, Kraków, Poland, January 7–9, 2013.

This paper describes several cross section measurements of electroweak boson production. This includes a measurement with jets in the final state. Other LHCb measurements cover further soft QCD-related topics including the forward energy flow [2], the charged particle multiplicities [3], the inclusive ϕ cross-section [4], the V^0 production ratios [5] and prompt K_S production [6]. These last analyses will not be described here.

2. Electroweak bosons at LHCb

Measurements of W, Z and low mass Drell–Yan production cross sections provide an important test of the Standard Model at the LHC energies. Predictions for these processes are available at next-to-next-to-leading order (NNLO). They have an uncertainty between 3 and 10% depending on the rapidity. The dominant theoretical uncertainty is due to the limited knowledge of the parton distribution functions. Precise measurements of the production cross sections by LHCb test the Standard Model, where predictions are most precise. Furthermore, precise measurements provide valuable input for the fitting of parton distribution functions. The measurements presented here cover the region $2.0 < \eta < 2.5$ common to ATLAS, CMS and LHCb as well as regions with $\eta > 2.5$ that are unique to LHCb.

Figure 1 shows the regions in the x–Q^2 plane probed by electroweak boson production in LHCb. Here x is the longitudinal momentum fraction carried by the interacting parton. Q^2 is the square of the four momentum

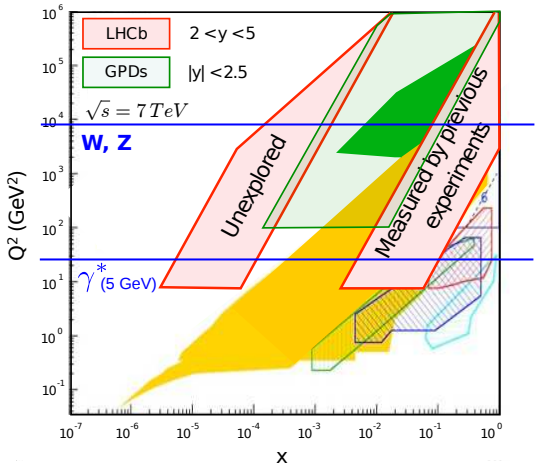

Fig. 1. The kinematic region x–Q^2 probed by the LHCb measurements of electroweak boson production. Underlaid are the regions probed by measurements of previous experiments as well as ATLAS and CMS (GPDs).

exchanged in the scattering process. For production processes at LHCb, the momenta of the two interacting partons are highly asymmetric. Such events include one parton at low-x and the other at high-x. Measurements of W and Z production at LHCb probe x values down to 1.7×10^{-4}. Measurements of the low mass Drell–Yan process are sensitive to x values of 8×10^{-6}. Figure 1 shows that the high-x region has been constrained by previous measurements. The low-x region, however, has only been probed at very low Q^2.

3. $pp \to Z \to l^+l^-$

LHCb has determined the Z production cross section in three leptonic decay channels ($\mu^+\mu^-$, e^+e^-, $\tau^+\tau^-$). All events are selected by requiring the single muon or the single electron trigger. The triggers have a threshold for the transverse momentum of 10 and 15 GeV/c, respectively. For all three measurements, the events are further selected to correspond to the fiducial region listed in Table I.

TABLE I

Fiducial region of the LHCb Z production measurements.

Dilepton invariant-mass	$60 < \mathrm{M}_{ll} < 120$ GeV/c^2
Pseudorapidity of lepton	$2 < \eta_l < 4.5$
Transverse momentum of lepton	$p_\mathrm{T} > 20$ GeV/c

The $Z \to \mu^+\mu^-$ measurement [7] is based on a 37 pb^{-1} dataset collected in 2010. Over 99% of the events selected for this measurement are signal events. The resulting dimuon invariant mass peak is shown in figure 2 (top).

The $Z \to e^+e^-$ measurement [8] is based on a dataset of 945 pb^{-1} collected in 2011. The selected events have a signal fraction of 95.5% with the main background caused by misidentified hadrons. The electron energy is estimated from the track momentum measurement, since the LHCb calorimeter saturates at high transverse energies. The invariant mass peak reconstructed from this data is shown in figure 2 (bottom). Due to bremsstrahlung, this peak is significantly broader than the one from the $Z \to \mu^+\mu^-$ measurement.

The third measurement [9] selects $Z \to \tau^+\tau^-$ events, where the τ decays into muons, electrons or hadrons. All final states are only partially reconstructed and the selected samples are contaminated by several background sources. The main backgrounds come from misidentified hadrons, misidentified leptons and $Z \to \mu^+\mu^-$ events. The signal fraction in the different samples is typically around 70%.

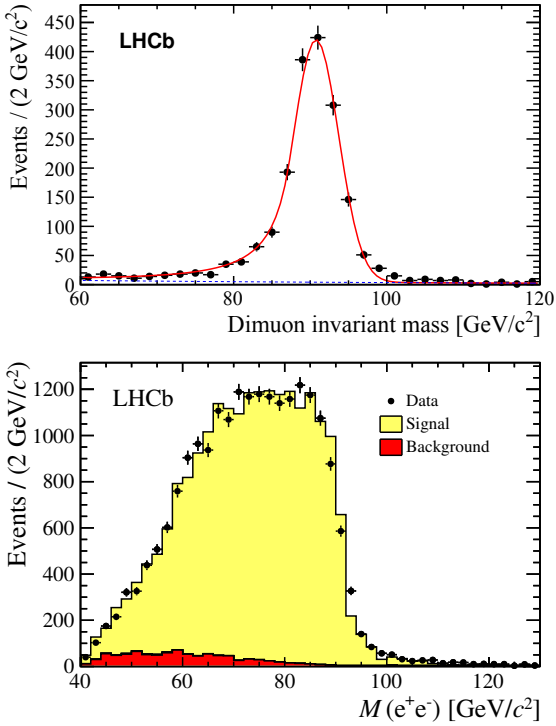

Fig. 2. Dilepton invariant mass peaks reconstructed in the $Z \to \mu^+\mu^-$ (top) and $Z \to e^+e^-$ (bottom) channels.

To determine the production cross section, the signal yield is corrected for the final state radiation. The corrected signal yield is then divided by the integrated luminosity and the different efficiencies. Most efficiencies for the three measurements are determined from data with a tag-and-probe method. The remaining efficiencies are estimated by comparing simulation and data. The uncertainty in the efficiency determination is the source of the dominant systematic uncertainty for the e and μ measurements. For the τ measurement, the uncertainty in the determination of the backgrounds dominates. Table II lists the three measured cross sections together with their uncertainties. The three measurements are consistent with each other and with NNLO predictions. The size of most systematic uncertainties is dominated by the statistics of the data samples used for the efficiency determination. These uncertainties will reduce significantly when all collected data are included.

TABLE II

Production cross section measured for the three decay channels of the Z boson. The first uncertainty is statistical, the second is the systematic uncertainty and the third is the luminosity uncertainty. For comparison, the theory prediction calculated by FEWZ [12] with the parton distribution functions from MSTW08 [13] is listed. Here, the second uncertainty is due to scale dependence while the first is due to the uncertainty of the parton distribution functions.

$\sigma_{pp\to Z\to ee}$	$76.0 \pm 0.8 \pm 2.0 \pm 2.6$ pb
$\sigma_{pp\to Z\to \mu\mu}$	$76.7 \pm 1.7 \pm 3.3 \pm 2.7$ pb
$\sigma_{pp\to Z\to \tau\tau}$	$71.4 \pm 3.5 \pm 2.8 \pm 2.5$ pb
$\sigma_{\text{FEWZ+MSTW08}}$	$74.7^{+1.6}_{-1.4} \pm 0.4$ pb

The $Z \to \mu^+\mu^-$ and the $Z \to e^+e^-$ analyses also measure the production cross section differentially in rapidity. In addition, the $Z \to e^+e^-$ analysis provides a measurement in ϕ^*, where ϕ^* is defined as

$$\phi^* \equiv \frac{\tan\left(\frac{\pi - |\Delta\phi|}{2}\right)}{\cosh\left(\frac{\Delta\eta}{2}\right)}.$$

Here, $\Delta\eta$ and $\Delta\phi$ are the differences between the leptons in pseudorapidity and azimuthal angles, respectively. ϕ^* is correlated with the transverse momentum but is less affected by the energy resolution. Figure 3 shows the

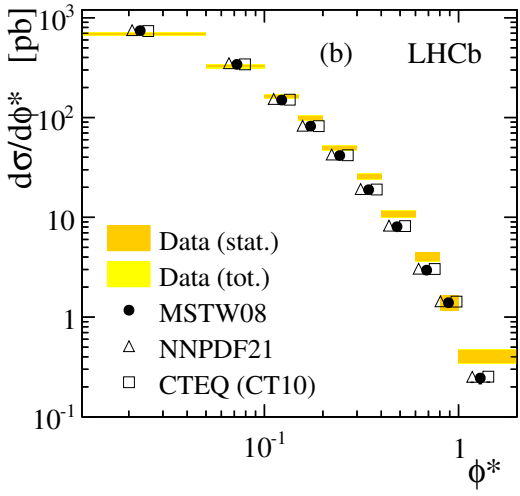

Fig. 3. Differential cross section for $pp \to Z \to ee$ as a function of ϕ^* (shaded histogram). NNLO QCD predictions are shown as points with error bars.

resulting distribution. The measurement is compared to NNLO predictions with three different sets of parton distribution functions. The measurement and predictions disagree for large ϕ^* as NNLO calculations ignore the effect of soft gluon radiation.

4. $pp \to Z \to \mu^+\mu^-$ + jets

The LHCb measurement of Z + jet production [10] uses the $Z \to \mu\mu$ final state with the selection described above. It is based on a dataset of 1 fb^{-1}. The jets are reconstructed in the pseudorapidity range $2 < \eta < 4.5$ using an anti-k_{T} clustering algorithm with a radius parameter $R = 0.5$. Each jet is required to have a transverse momentum above 10 GeV/c and to be isolated from any muon. The jet energy is calibrated using simulation and cross-checked in data with a typical uncertainty of 3%. This, together with the uncertainty of the jet energy resolution, is the source of the dominant systematic uncertainty.

The ratio of events with a Z boson and at least one jet to all events with a Z boson is measured to be $0.229 \pm 0.006(\mathrm{stat}) \pm 0.009(\mathrm{syst})$. The prediction from theory is $0.212^{+0.006}_{-0.009}(\mathrm{PDF}) \pm 0.016(\mathrm{theory})$. The theory expectation is calculated using FEWZ at $\mathcal{O}(\alpha_{\mathrm{s}}^2)$. Again, the second uncertainty is due to scale dependence and the first is due to the uncertainty in the parton distribution functions. Figure 4 shows this ratio differentially in five bins of Z rapidity. As can be seen the data agree with the theoretical predictions.

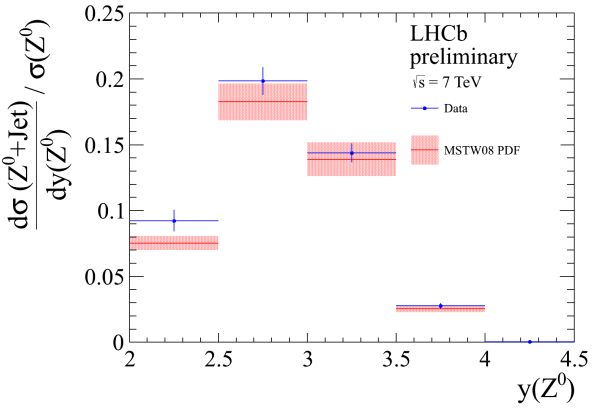

Fig. 4. The normalised Z rapidity distribution measured in Z + jet events in data (blue points), with the FEWZ+MSTW08 predictions overlaid (the grey/red line gives the central value).

5. $pp \to W \to \mu\nu$

The $W \to \mu\nu$ measurement [7] uses the same dataset as the $Z \to \mu^+\mu^-$ analysis and similar selection requirements for the muons. Adding requirements on calorimetry deposits and consistency with the primary vertex helps to reduce backgrounds. Moreover, events with two muons in the LHCb acceptance are excluded. The selection efficiency is evaluated from $Z \to \mu^+\mu^-$ events by masking each of the muons in turn. Such masked events mimic the presence of a neutrino and fake a $W \to \mu\nu$ decay. Excellent agreement between true and faked decays is observed for all variables.

The selected W^+ and W^- events have a signal fraction of $78 \pm 2\%$. The signal yield is determined by fitting the muon transverse momentum spectra in data in five bins of muon pseudorapidity. A template fit is performed considering four sources for background: K/π decay in flight, Drell–Yan decays into muons, W and Z decays into τ and misidentified hadrons. Where possible, these template shapes are taken from data.

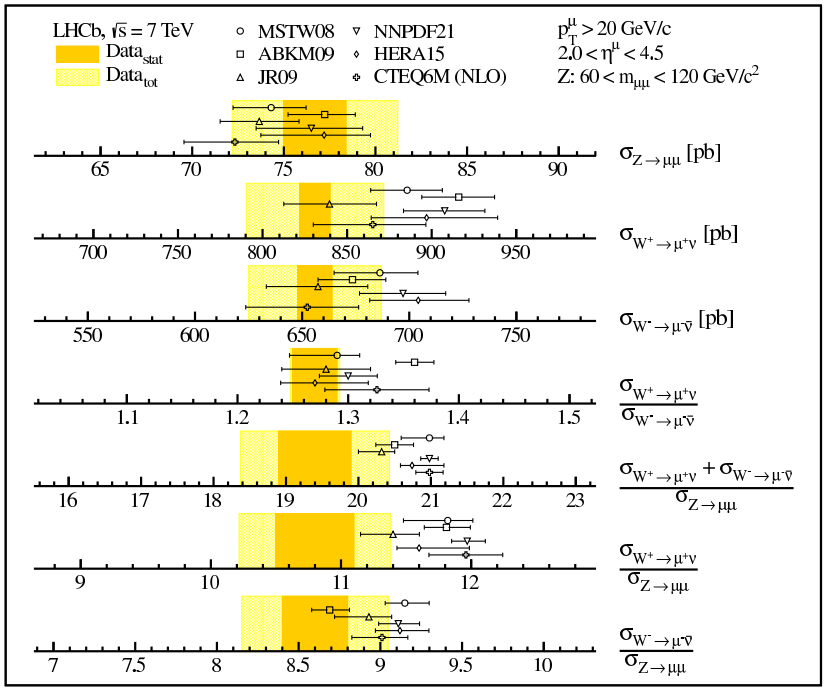

Fig. 5. Measurements of the Z, W^+ and W^- cross sections and ratios, data are shown as bands with the statistical (dark shaded/orange) and total (light hatched/yellow) uncertainties. The measurements are compared to NNLO and NLO predictions.

Figure 5 summarises the measurements of the inclusive production cross sections $\sigma_{pp\to W\to\mu\nu}$ and $\sigma_{pp\to Z\to\mu\mu}$. For the $\sigma_{W^+\to\mu^+\nu}/\sigma_{W^-\to\mu^-\nu}$ ratio, most of the systematic uncertainties cancel, leading to a very precise measurement. All measurements are in agreement with NNLO predictions. Besides the luminosity uncertainty, the uncertainty of the efficiencies, the template shapes and the selection contribute significantly to the systematic error.

6. Low mass Drell–Yan

The low mass Drell–Yan measurement [11] is performed differentially both in rapidity and invariant mass of the dimuons. It covers the dimuon invariant mass range from 5 to 120 GeV/c^2. The region 9 to 10.5 GeV/c^2, containing the Upsilon resonance, is excluded. The measurement is based on the dataset of 37 pb^{-1} collected in 2010. Muons are required to have a transverse momentum larger than 3 GeV/c and a pseudorapidity in the range of $2.0 < \eta < 4.5$.

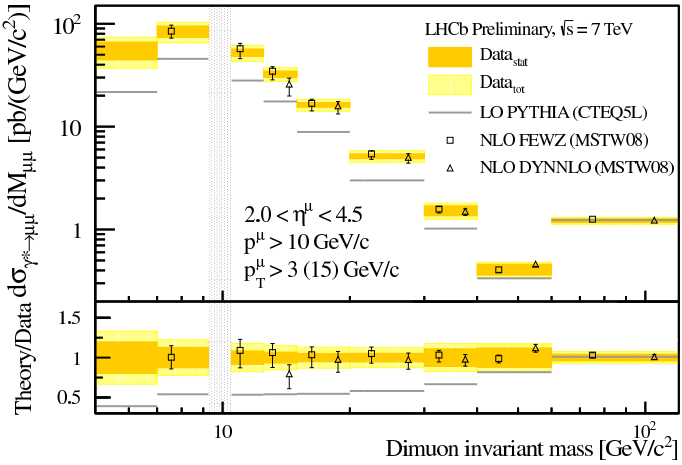

Fig. 6. Differential cross section for Drell-Yan production as a function of dimuon invariant mass. Superimposed are the PYTHIA predictions and the NLO predictions from FEWZ and DYNNLO. The shaded vertical band corresponds to the mass region of the Υ resonance which is not included in the measurement. The lower plot shows the ratio of the predictions or the uncertainties to the data.

The signal yield is determined in bins of the dimuon invariant mass. In each bin, a template fit to the minimum muon isolation is performed. The muon isolation is defined as the fraction of the transverse momentum in the muon-jet carried by the muon. The muon-jet is the jet which contains the muon. The background sources relevant for the fit are misidentified hadrons, muons from heavy flavour decays and, below 9 GeV/c^2, events

from the tail of the Upsilon resonance. Where possible, the template shapes are determined from data. The signal fraction obtained is below 10% in the lowest mass range and increases to over 99% in the Z region. The fit dominates the systematic uncertainties in the low mass bins. At high masses, the uncertainties of the efficiency calculations dominate. As in the $Z \to l^+l^-$ measurement, most efficiencies are determined from data.

The Drell–Yan production cross section, differentially as a function of the invariant mass, is shown in figure 6. NLO predictions are only available for masses larger than 7 GeV/c^2 for FEWZ and 12.5 GeV/c^2 for DYNNLO [14]. Where available, the NLO predictions are in reasonable agreement with the measurement. The PYTHIA [15] predictions agree in shape but are too low in normalisation.

7. Summary and outlook

Since the LHCb detector is fully instrumented in the forward region, electroweak boson production explores a unique region in x and Q^2. Using the data acquired in 2010 and 2011, LHCb has measured W, Z and Drell–Yan production cross sections in several channels. Except for the high ϕ^* region, the results are in agreement with theoretical predictions.

In the near future, the remaining analyses will be updated with the full 2011 dataset, followed by the inclusion of the 2012 data. The higher centre of mass energy in 2012 will allow the kinematic reach of the measurements to be extended to even lower values of x.

REFERENCES

[1] A. Augusto Alves *et al.* [LHCb Collaboration], *JINST* **3**, S08005 (2008).

[2] R. Aaij *et al.* [LHCb Collaboration], `arXiv:1212.4755 [hep-ex]`.

[3] R. Aaij *et al.* [LHCb Collaboration], *Eur. Phys. J.* **C72**, 1947 (2012) [`arXiv:1112.4592 [hep-ex]`].

[4] R. Aaij *et al.* [LHCb Collaboration], *Phys. Lett.* **B703**, 267 (2011) [`arXiv:1107.3935 [hep-ex]`].

[5] R. Aaij *et al.* [LHCb Collaboration], *J. High Energy Phys.* **1108**, 034 (2011) [`arXiv:1107.0882 [hep-ex]`].

[6] R. Aaij *et al.* [LHCb Collaboration], *Phys. Lett.* **B693**, 69 (2010) [`arXiv:1008.3105 [hep-ex]`].

[7] R. Aaij *et al.* [LHCb Collaboration], *J. High Energy Phys.* **1206**, 058 (2012) [`arXiv:1204.1620 [hep-ex]`].

[8] R. Aaij *et al.* [LHCb Collaboration], *J. High Energy Phys.* **1302**, 106 (2013) [`arXiv:1212.4620 [hep-ex]`].

[9] R. Aaij *et al.* [LHCb Collaboration], *J. High Energy Phys.* **1301**, 111 (2013) [arXiv:1210.6289 [hep-ex]].

[10] R. Aaij *et al.* [LHCb Collaboration], LHCb-CONF-2012-016.

[11] R. Aaij *et al.* [LHCb Collaboration], LHCb-CONF-2012-013.

[12] R. Gavin, Y. Li, F. Petriello, S. Quackenbush, *Comput. Phys. Commun.* **182**, 2388 (2011) [arXiv:1011.3540 [hep-ph]].

[13] A.D. Martin, W.J. Stirling, R.S. Thorne, G. Watt, *Eur. Phys. J.* **C63**, 189 (2009) [arXiv:0901.0002 [hep-ph]].

[14] S. Catani, M. Grazzini, *Phys. Rev. Lett.* **98**, 222002 (2007) [arXiv:hep-ph/0703012].

[15] T. Sjöstrand, S. Mrenna, P.Z. Skands, *J. High Energy Phys.* **0605**, 026 (2006) [arXiv:hep-ph/0603175].